MOLYBDENUM TRIOXIDE THIN FILMS DOPED WITH GOLD NANOPARTICLES GROWN BY A SEQUENTIAL METHODOLOGY: PHOTOCHEMICAL METAL-ORGANIC DEPOSITION (PMOD) AND DC-MAGNETRON SPUTTERING

C. CASTILLO[1], G. BUONO-CORE[1], C. MANZUR[1], N. YUTRONIC[2], R. SIERPE[2], G. CABELLO[3], B. CHORNIK[4].*

[1]*Instituto de Química, Pontificia Universidad Católica de Valparaíso, Valparaíso, Chile.*
[2]*Departamento de Química, Facultad de Ciencias, Universidad de Chile.*
[3]*Departamento de Ciencias Básicas, Facultad de Ciencias, Universidad del Bío-Bío, Chillán, Chile*
[4]*Departamento de Física, Facultad de Ciencias Físicas y Matemáticas, Universidad de Chile.*

ABSTRACT

Gold nanoparticles (AuNPs) were deposited by DC-magnetron sputtering onto molybdenum trioxide (MoO_3) thin films grown by Photochemical Metal-Organic Deposition (PMOD) on Si(100) and borosilicate glass substrates. The chemical, optical and morphology properties of the films were studied by UV/Vis Spectroscopy, Scanning Electron Microscopy (SEM), X-Ray Photoelectron Spectroscopy (XPS), and X-Ray Diffraction (XRD). SEM revealed that AuNPs formed after 5 s of sputtering. AuNPs are spherical and have both an average diameter of 18 nm and a relatively narrow size distribution. As the deposition time increases, larger structures are formed by an aggregation of AuNPs. XPS studies of the AuNP/MoO_3 films on Si(100) showed the presence of Mo(VI) and Mo(V), which indicated that the films were primarily non-stoichiometric molybdenum oxides. The occurrence of oxygen vacancies in the substrate play an important role to stabilize the AuNPs.

Keywords A. oxides, A. thin films, A. nanostructures, B. sputtering; C. x-ray diffraction, C. photoelectron spectroscopy

1. INTRODUCTION

Unique properties can be achieved by reducing a material to the nanometer scale. Metal nanoparticles (MNPs) present attractive optical, electronic, magnetic and chemical properties, among others, which are not displayed in the bulk state [1,2]. Gold nanoparticles (AuNPs) are the most stable MNP; they can be synthesized with different sizes and shapes; and they are easily functionalized with diverse ligands [3]. AuNPs have numerous applications in nanomedicine [4,5], biotechnology [6], microelectronics [7], optics [8-10], gas sensing [11-13] and catalysis [14-20].

AuNPs have been prepared using various approaches that can be divided into physical and chemical methods. Included among the chemical methods are reduction [21], photochemistry using UV irradiation [22,23], photochemistry using X-ray irradiation [24], sonochemistry [25,26], and sonoelectrochemistry [27]. A physical method that can be used is cathodic deposition using magnetron sputtering. This physical method has several advantages over chemical syntheses, such as a lack of surface contamination from solvent or precursor molecules, which may be important for subsequent assays and/or applications. Furthermore, physical deposition is cheaper and faster and does not damage the environment [28-30].

Gold catalysts with selected support materials can efficiently promote many reactions that normally occur at much higher temperatures or with lower selectivity when catalyzed by other metals. It has been shown that AuNPs supported on metal oxides exhibit unique activity at room temperature because of a meta-stable interatomic bonding between gold atoms [31]. It has been shown that substrates such as ceria [32], titania [33,34] and titanates [35] can stabilize AuNPs in which oxygen vacancies play an important role in the stabilizing effect. It is generally accepted that interfaces provide adequate sites for chemical reactions, and metallic Au surfaces are required as reservoirs for a determined reactant [36,37]. Gold nanoparticles also play an important role in the development of chemical and biological sensors. A sensor usually has two functional components: one component selectively binds with the analyte, and the other provides transduction of this interaction into a detectable signal [38]. Considering the chromogenic properties of molybdenum oxide on the one hand and the catalytic properties of gold nanoparticles on the other, a binary system that is formed by molybdenum oxide coated with gold nanoparticles could potentially be of use in the field of catalysis and/or in the fabrication of new specific sensors. For example, it has been found that the UV-light coloration performance of MoO_3 thin films can be enhanced by modification of the MoO_3 surface with gold nanoparticles [39]. In this work, the synthesis and characterization of a AuNPs/MoO_3 system is examined. To synthesize the support material, i.e., molybdenum oxide, a pure photochemical deposition method such as PMOD is used, followed by the synthesis of AuNPs using a DC-magnetron sputtering method. The synthesis of MoO_3 thin films deposited onto Si(100) by PMOD, has been described at length in a previous publication from our group [40].

2. Materials and methods

2.1 General procedure

X-ray photoelectron spectra (XPS) were recorded on an XPS-Auger Perkin Elmer electron spectrometer Model PHI 1257 in an ultra-high vacuum chamber, with a hemispherical electron energy analyzer and an Al Kα X-ray source ($h\nu$ = 1486.6 eV). The pressure of the spectrometer during data acquisition was maintained at 10^{-9} mbar. The binding energy (BE) scale was calibrated using adventitious carbon set to 284.8 eV. The accuracy of the BE scale was ± 0.1 eV. High resolution spectra were fitted using Gaussian–Lorentzian curves and a Shirley background [41]. The approximate composition of the surface was determined for each element by dividing the individual peak area, after appropriate background subtraction, by their respective atomic sensitivity factors (ASF). XRD patterns were obtained using a Bruker D8 Advance diffractometer. The X-ray source was Cu 40 kV/40 mA. The surface plasmon resonance (SPR) effect of AuNPs on Mo oxide films was examined by solid-state UV-Vis spectrophotometry from 200 to 800 nm. References of barium sulfate ($BaSO_4$) and a Mo oxide thin film deposited onto quartz were used. The equipment used was a Shimadzu UV-2450 spectrophotometer with an integrating sphere ISR-2200 and controlled by the UVProbe software version 1.10. First, the diffuse reflectance of the samples was measured; then, via the Kubelka-Munk mathematical transformation, all absorbances were obtained. Scanning electron microscopy (SEM) images were obtained on a LEO 1420VP at an accelerating voltage of 25 kV and coupled to an energy dispersive analysis instrument, Oxford 7424 model. For FE-SEM images a Leo Zeiss Supra 35-VP model was used with accelerating voltages of 15 kV and 2 kV. Samples were prepared by coating the molybdenum trioxide thin films with Au nanoparticles through the sputtering method with deposition times of 1, 2, 3, 4, 5 and 20 s. The total count of Au nanoparticles on the oxide was evaluated using SEM images. A histogram was built with the Origin 8 software with a Gaussian fit analysis. Mathematical treatments of the average sizes with standard deviations were calculated by this program.

2.2 Materials

A gold target (Quorum Technologies Ltd.) was cleaned with ethanol, acetone, and deionized water and dried at 80 °C prior to use. Molybdenum thin films were deposited onto Si(100) and borosilicate glass.

2.3 Synthesis of MoO_3 thin films.

Post-annealing of the MoO_3 films was carried out at 400 °C for 2 h under a continuous flow of synthetic air in a programmable Lindberg tube furnace and then allowed to slowly return to room temperature.

2.4 Synthesis of AuNPs on MoO_3 thin films.

AuNPs were deposited onto MoO_3 thin films by Magnetron Sputtering

 e-mail: gbuonoco@ucv.cl

with a DC diode sputtering single source. The equipment used was a Magnetron Sputter Coater Pelco SC-6 with a gold target (99.99%). Pre-deposited MoO_3 thin films were introduced into the vacuum chamber at a pressure of 0.05 mbar. Argon was used for sputtering with an ionization current of 25 mA and the gold foil as the cathode. The deposition times were 1, 2, 3, 4, 5 and 20 s, and the MoO_3 film was maintained at constant pressure.

3. RESULTS AND DISCUSSION

3.1 Synthesis and characterization of Au NPs onto MoO_3 thin films

The formation of AuNPs on the MoO_3 surface was confirmed by monitoring the UV/Vis absorption band associated with the surface plasmon resonance (SPR). SPR absorption band measurements provide information about the presence and estimated size of the AuNPs on the oxide film. This method was used to evaluate the effects of different sputtering times on the deposition of gold NPs and to determine the optimum deposition time [1,28]. Surface plasmon absorption spectra of spherical gold nanoparticles prepared by DC-sputtering for different deposition times are shown in Fig 1. As observed from the figure, the absorption spectrum maximum is shifted from 560 nm for NPs produced by 3 s of sputter depositing to 585 nm for NPs produced during a 5-s deposition.

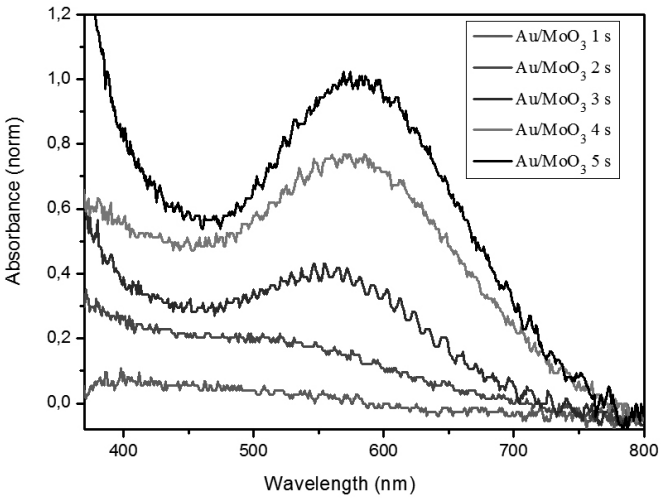

Fig. 1 UV/Vis surface plasmon resonance absorption of gold nanoparticles deposited onto MoO_3 thin films by DC-magnetron sputtering with different deposition times.

The bathochromic shift is also accompanied by a broadening of the band and an increase in the intensity, which is associated with an increase in the diameter and number of the gold particles. This could also result from NP aggregation or an interparticle coupling phenomenon produced by the proximity of metal NPs [42]. As a consequence, NPs that are arranged side by side behave as a single, larger structure with a collective effect on the plasmon resonance. Longer sputtering times were evaluated; however, the surface plasmon effect was lost, likely because of an excess of AuNPs.

SEM studies showed that nanoparticles deposited under these conditions have an apparent spherical shape and were homogeneously dispersed on the surface layer of oxide (Fig. 2a). Increasing the time of sputtering produces an increase in the size of the NPs. The average size of the Au particles that formed using a 5-s deposition, as determined by a size distribution study of the SEM image, was measured to be 18 nm, with a relatively narrow size distribution (histogram Fig. 2c). SEM images and their respective histograms show dispersity of nanostructure sizes. Therefore, 5 s corresponds to the optimum deposition time. As previously discussed, the increase in bandwidth and the absorption band shift towards higher wavelengths are the result of a dipolar coupling between closely spaced particles [28,43,44]. NP aggregations on the oxide surface are observed for samples that were subjected to 20 s of sputter depositing, as shown in the SEM image (Fig. 2b), and have an average particle size of 460 nm, as determined by the particle size distribution (histogram, Fig. 2d).

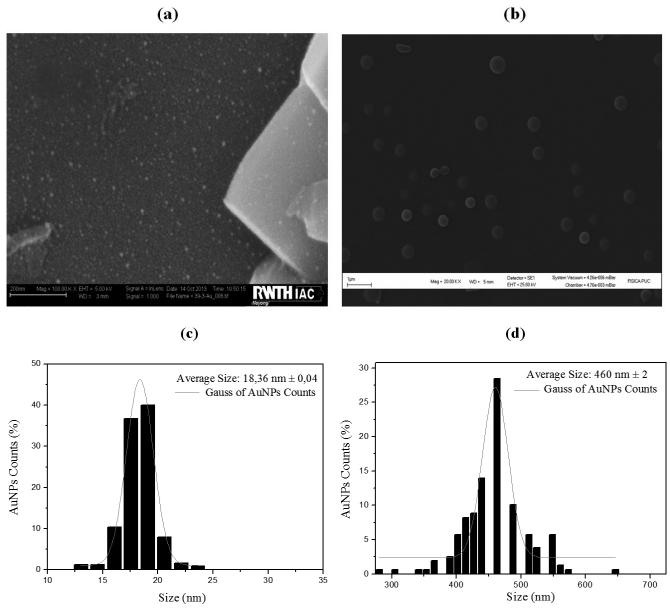

Fig. 2 SEM images of MoO_3 films doped with AuNPs **(a)** deposition time = 5 s / Mag. = 100.000x **(b)** deposition time = 20 s / Mag. = 20,000x. Histograms of particle size distribution for the AuNP/MoO_3 films **(c)** deposition time = 5 s and **(d)** deposition time = 20 s

To obtain information concerning the chemical state of the AuNPs, the samples were characterized by XPS. The low-resolution XPS spectrum of a sample that contained 18-nm AuNPs (Fig. 3) shows the characteristic signals of O and Mo for the support and the signal of Au for the AuNPs, thus confirming the presence of metal in the film. The signal intensity was significantly lower for Mo and O than for Au, which was the predominant species in the test area. The presence of the C 1s signal is associated with the adsorbed carbon impurities on the surface of the film.

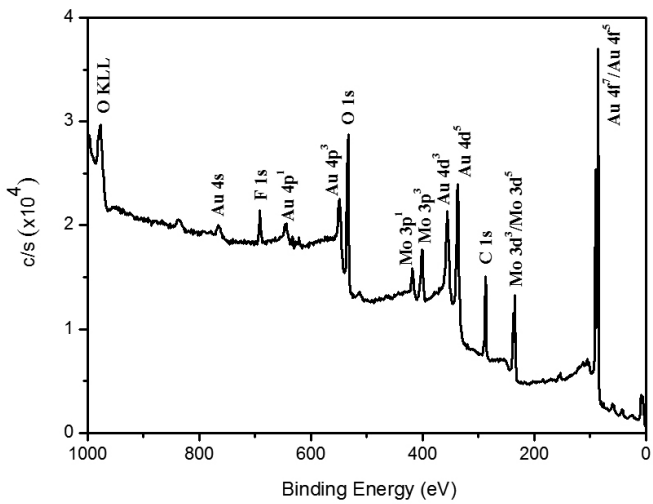

Fig. 3 Wide-scan XPS spectrum of an Au/MoO_3 thin film (sputtering time = 5 sec).

The high-resolution spectra of the Au 4f lines (Fig. 4a) show one doublet located at 83.9 and 87.5 eV, which correspond to Au $4f_{7/2}$ and Au $4f_{5/2}$, respectively. These values are in agreement with the data reported by other authors [45] and indicate that the chemical species present in the film corresponds to Au (0), without other satellite signals [45-49].

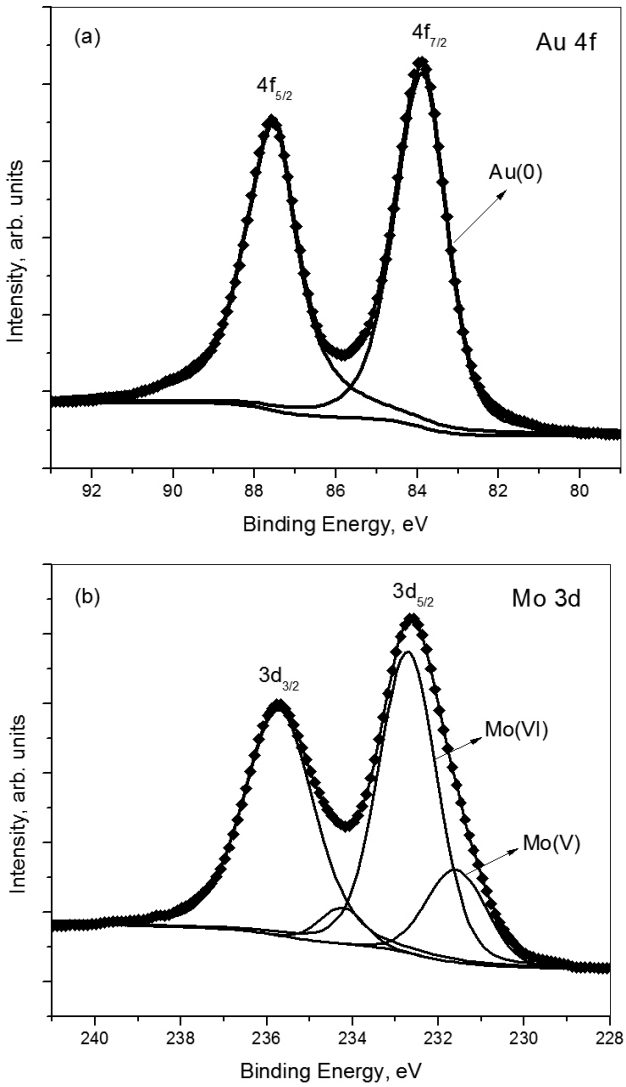

Fig. 4 High-resolution XPS spectra of Au/MoO_3 films (a) Au 4f and (b) Mo 3d.

For the case of Mo 3d (Fig. 4b, Table 1) the predominant species (> 90%) corresponds to Mo (VI), with binding energies of 232.7 eV for Mo $3d_{5/2}$ and 235.7 eV for Mo $3d_{3/2}$ [50-54]. The presence of signals assigned to Mo(V) species at 231.6 eV for Mo $3d_{5/2}$ and 234.4 eV for Mo $3d_{3/2}$, could be explained by the over-irradiation of the photodeposited oxide or the catalytic action of the noble metal on the MoO_3 surface. Finally, the O 1s peak shows the same composition as that determined for MoO_3 films without Au doping, with an oxygen contribution from the oxide in the film and from adsorbed OH [41].

Table 1 Standard binding energies for Mo 3d photoelectron peaks associated with different oxidation states [50].

Oxidation State	Standard Values (±0.1 eV)		Experimental Values (eV)	
	Mo $3d_{5/2}$	**Mo $3d_{3/2}$**	**Mo $3d_{5/2}$**	**Mo $3d_{3/2}$**
Mo(VI)	232.5	235.7	232.7	235.7
Mo(V)	231.5	234.7	231.6	234.4
Mo(IV)	230.1	233.3		
Mo(III)	229.3	232.5		
Mo(II)	228.4	232.6		
Mo^0	227.7	230.9		

The crystal structure of the AuNPs was studied by XRD. The diffractogram of an Au/MoO_3 film with 470 nm NPs (Fig. 5a) clearly shows the presence of orthorhombic α-MoO_3 preferentially oriented along the [020] axis [55-57], but no signals attributed to the gold NPs can be observed. This is likely due to a combination of factors, including the small particle size, the small grain size, and the relatively low concentrations of Au relative to MoO_3. However, an XRD diffractogram using a grazing incidence angle (Fig. 6b) shows diffraction peaks at 2θ = 38.2° for the flat Au (111), 2θ = 44.2° for Au (200) and 2θ = 64.9° for Au (220), in accordance with the literature (JCPDS No. 04-0784). These results suggest that 470 nm AuNPs would exhibit a face centered cubic (fcc) structure [24,58].

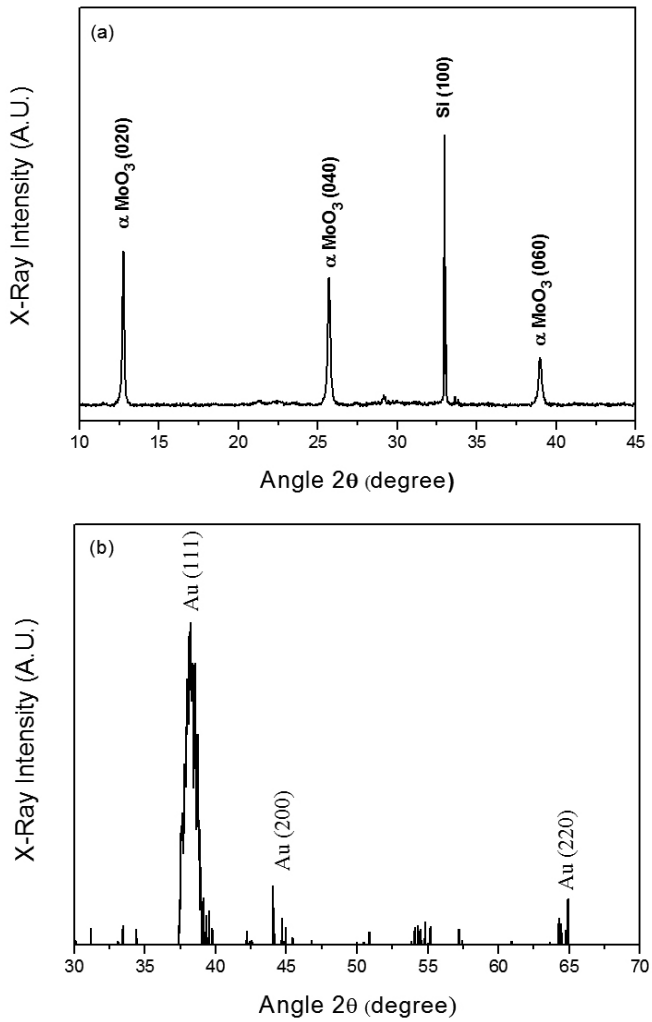

Fig. 5 XRD spectra of a MoO_3 film (annealed at 400°C for 2 h) doped with 470 nm AuNPs deposited by magnetron sputtering, (a) measured with the Bragg-Brentano instrumental function and (b) with grazing incidence.

3.2 Optical Properties

The variation in absorbance spectra of the MoO_3 thin films doped with AuNPs is indicative of changes in the optical properties of the films. The optical band gap of the films can be estimated from the Tauc equation using their absorption spectra measured at room temperature. From solid-state band theory, the relation between the absorption coefficient α and the energy of the incident light *hv* is given by

$$(\alpha h\nu) = A(h\nu - E_g)^n$$

where A is the probability parameter for the transition and E_g is the optical band gap energy. For allowed direct transitions, the coefficient n = 2, and for allowed indirect transitions, n = 1/2. The values of E_g are estimated from the intersection of the extrapolated linear part of the $(\alpha h\nu)^2$ curves with the

energy axis (Fig. 6). The optical band gaps computed from the above relation are estimated to be 3.60 and 3.21 eV (when n = 2) for undoped and AuNP doped MoO_3 films, respectively. The value of the optical band-gap energy for the undoped MoO_3 film is in good agreement with the reported values for this non-stoichiometric oxide [53,54,57]. Once MoO_3 films are doped with AuNPs, the band gap decreases to 3.21 eV. A possible explanation is that the deposition of catalytic metal nanoparticles forms additional intermediate electronic states in the metal oxide, which reside between the top of the valence band and the bottom of the conduction band [13,59].

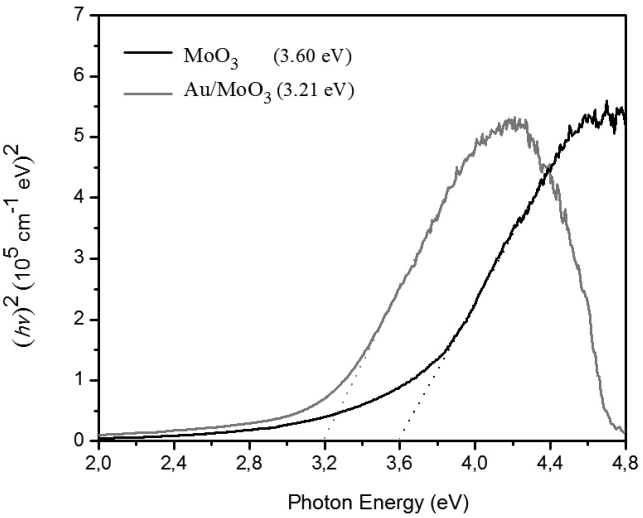

Fig. 6 Optical Band-Gap of MoO_3 thin films undoped and doped with AuNPs.

4. CONCLUSIONS

The results of our studies demonstrate that the deposition of gold nanoparticles onto MoO_3 films can be successfully achieved by a combination of PMOD and DC-magnetron sputtering methods. AuNPs with an average size of 18 nm formed after 5-s sputter depositing, and their size was directly related to the time used in the sputtering process. Increased deposition time caused significant particle growth, which reached 460 nm after a 15-s deposition. XRD using grazing incidence angle indicated that the Au in the Au/MoO_3 films exhibited a monocrystalline face-centered cubic structure. The gold possessed a single oxidation state, Au (0), as determined by high-resolution XPS analysis. XRD analysis also showed the presence of orthorhombic α-MoO_3 with a (020) preferential orientation. XPS surface analysis demonstrated the different contributions of Mo(VI) and Mo(V) oxidation states present in the thin film. Finally, gold doping caused a decrease in the MoO_3 optical bandgap, which was probably due to the formation of intermediate electronic states. The gasochromic performance of the AuNP doped MoO_3 films towards H_2 gas is currently being investigated by our group. We expect that the deposition of Au nanoparticles on the MoO_3 thin films will significantly improve the gasochromic properties of such films by increasing the sensitivity to H_2, improving the dynamic optical performance, and lowering the operating temperature.

ACKNOWLEDGMENTS

This research was supported by FONDECYT, Chile (Project No.1110439) and Pontificia Universidad Católica de Valparaíso (Project D.I. No. 125.756/11). C. Castillo thanks CONICYT, Chile for a doctoral fellowship and doctoral thesis support (Project No 24110020). We also thank Dr. Michael Noyong of Institut für Anorganische Chemie at Aachen, for preparing the SEM images.

REFERENCES

[1] M. Daniel, D. Astruc, Chem. Rev. 104 293-346 (2004).
[2] P. Zhao, N. Li, D. Astruc, Coord. Chem. Rev. 257 638-665 (2013).
[3] M. Grzelczak, J. Perez-Juste, P. Mulvaney, L.Liz-Marz, Chem. Soc. Rev. 37 1783-1791 (2008).
[4] Juan J. Giner-Casares, Luis M. Liz-Marzán, Nano Today 9 365-377 (2014).
[5] A.K. Khan, R. Rashid, G. Murtaza, A. Zahra, Trop. J. Pharm. Res. 13 1169-1177 (2014).
[6] A. Liu, B. Ye, Clin. Lab. 59 23-36 (2013).
[7] R. Andres, T. Bein, M. Dorogi, S. Feng, J. Henderson, C. Kubiak, W. Mahoney, R. Osifchin, R. Reifenberge, Science 272 1323 (1996).
[8] T. Okamoto, I. Yamaguchi, J. Phys. Chem. B 107 10321-10324 (2003).
[9] I. Sosa, C. Noguez, R. Barrera, J. Phys. Chem. B 107 6269-6275 (2003).
[10] J. Novak, L. Brousseau, F. Vance, R. Johnson, B. Lemon, J. Hupp, D. Feldheim, J. Am. Chem. Soc. 122 12029-12030 (2000).
[11] M. Ando, T. Kobayashi, S. Iijima, M. Haruta, J. Mater. Chem. 7 1779–1783 (1997).
[12] M. Ando, T. Kobayashi, S. Iijima, M. Haruta, Sens. Actuators B 96 589-595 (2003).
[13] M. Ahmad, A. Sadek, M. Yaacob, D. Anderson, G. Matthews, V. Golovko, W. Wlodarski, Sens. Actuators B 179 125-130 (2013).
[14] T. Takei, K. Akita, I. Nakamura, T. Fujitani, M. Okumura, K. Okazaki, J.H. Huang, T. Ishida, M. Haruta, Adv. Catal. 55 1-126 (2012).
[15] C. Della Pina, E. Falletta, L. Prati, M. Rossi, Chem. Soc. Rev. 37 2077-2095 (2008).
[16] A. Corma, H. Garcia, Chem. Soc. Rev. 37 2096-2126 (2008).
[17] Y. Zhang, X.J. Cui, F. Shi, Y. Deng, Chem. Rev. 112 2467-2505 (2012).
[18] M. Stratakis, H. Garcia, Chem. Rev. 112 4469-4506 (2012).
[19] S.E. Davis, M.S. Ide, R.J. Davis, Green Chem. 15 17-45 (2013).
[20] Y. Mikami, A. Dhakshinamoorthy, M. Alvaro, H. García, Catal. Sci. Technol. 3 58-69 (2013).
[21] D.V. Leff, P.C. Ohara, J.R. Heath, W.M. Gelbart, J. Phys. Chem. 99 7036-7041 (1995).
[22] M. Kaushik, Z.L. Wang, P. Tarasankar, J. Photoch. Photobio. A 140 75 (2001).
[23] T.K. Sau, P. Anjali, N.R. Jana, Z.L. Wang, P. Tarasankar, J. Nanopart. Res. 3 257-261 (2001).
[24] N. Long, L. Vu, C. Kiem, S. Doanh, C. Nguyet, P. Hang, N. Thien, L. Quynh, J. Phys. Conf. Ser. 187 012026 (2009).
[25] O. Kenji, M. Yoshiteru, T.A. Yamamoto, M. Yasuaki, N.Yoshio, Mater. Lett. 61 3429 (2007).
[26] L. Cuncheng, C Weiping, K. Caixia, F. Ganhua, Z. Lide, Mater. Lett. 58 196 (2003).
[27] W. Liping, M. Wei, N. Dandan, D. Junwei, W. Ying, T. Yifeng, Electrochem. Commun. 10 673 (2008).
[28] L. Barrientos, N. Yutronic, F. del Monte, M. Gutiérrez, P. Jara, New. J. Chem. 31 1400-1402 (2007).
[29] G. Veith, A. Lupini, S. Pennycook, G. Ownby, N. Dudney, J. Catalysis 231 151-158 (2005).
[30] P. Kelly, R. Armell, Vacuum 56(3) 159-172 (2000).
[31] D.B. Akolekar, K. Bhargava, G. Foran, M. Takahashi, J. Mol. Catal. A-Chem. 238 78-87 (2005).
[32] M. Baron, O. Bondarchuk, D. Stacchiola, S. Shaikhutdinov, H.-J. Freund, J. Phys. Chem. C, 113, 6042–6049 (2009).
[33] S. Lee, C. Fan, T. Wu, S. L. Anderson, Surface Science 578 5–19 (2005).
[34] Á. Kukovecz, G. Pótári, A. Oszkó, Z. Kónya, A. Erdőhelyi, J. Kiss, Surface Science 605 1048–1055 (2011).
[35] P. Pusztai, R. Puskás, E. Varga, A. Erdohelyi, A. Kukovecz, Z. Konya, J. Kiss, Phys. Chem. Chem. Phys. 16 26786 (2014)
[36] M. Haruta, Chem. Record 3 75 (2003).
[37] M. Okumura, T. Akita, M. Haruta, X Wang, O. Kajikawa, O. Okada, Appl. Catal. B: Environmental 41- 43(2003).
[38] K. Saha , S.S. Agasti , C. Kim, X. Li , M. Vincent, Chem. Rev. 112(5) 2739-2779 (2012) .
[39] T. He, Y. Ma, Y. Cao, J. Peng, X. Zhang, W. Yang, J. Yao, Langmuir 17: 8024-8027 (2001).
[40] G.E. Buono-Core, A. Klahn, C. Castillo, E. Muñoz, C. Manzur, G. Cabello, B. Chornik, J. Non-Cryst. Solids 387 21-27 (2014).
[41] D.A. Shirley, Phys. Rev. B 5 4709-4714 (1972).
[42] Y. Hatakeyama, K. Onishi, K. Nishikawa, RSC Advances 1 1815-1821 (2011).
[43] K. Su, Q. Wei, X. Zhang, J. Mock, D. Smith, Nano Lett. 3 1087-1090 (2003).
[44] S. Ghosh, T. Pal, Chem. Rev. 107 4797-4862 (2007).
[45] R.G. Palgrave, I.P. Parkin, Chem. Mater. 19 4639-4647 (2007).
[46] H. Wei, J. Li, J. Zheng, H. Su, X. Wang, Inorg. Chim. Acta 427 33-40 (2015).
[47] M. Casaletto, A. Longo, A. Martorana, A. Prestianni, A. Venezia, Surf. Interface Anal. 38 215-218 (2006).

[48] L. Ono, B. Roldan-Cuenya, J. Phys. Chem. C 112 4676-4686 (2008) .
[49] N. Turner, A. Single, Surf. Interface Anal. 15 215-222 (1990).
[50] S. Sunu, E. Prabhu, V. Jayaraman, K. Gnanasekar, T. Seshagiri, T. Gnanasekaram, Sens. Actuators B 101 (2004) 161-174.
[51] O. Hussain, K. Rao, Mater. Chem. Phys. 80 638-646 (2003).
[52] R. Cardenas, J. Torres, J. Alfonso, Thin Solid Films 478 146-151 (2005).
[53] J. Dupin, D. Gonbeau, P. Vinatier, A. Levasseur, Phys. Chem. Chem. Phys. 2 1319-1324 (2000).
[54] A. Bouzidi, N. Benramdane, H. Tabet-Derraz, C. Mathieu, B. Khelifa, R. Desfeux, Mater. Sci. Eng. B 97 5-8 (2003).
[55] G.E. Buono-Core, G. Cabello, A. Klahn, A. Lucero, M.V. Nuñez, B. Torrejón, C. Castillo, Polyhedron 29 1551-1554 (2010).
[56] T. Chiang, H. Yeh, J. Alloys Compd. 585 535-541 (2014).
[57] M. Dhanasankar, K. Purushothaman, G. Muralidharan, Appl. Surf. Sci. 257 2074-2079 (2011).
[58] Y. Chen, X. Gu, C. Nie, Z. Jiang, Z. Xie, Chem. Commun. 4181-4183 (2005).
[59] D. Kaczmarek, J. Domaradzki, E. Prociow, T. Berlicki, K. Prociow, Opt. Mater. 31 1337-1339 (2009).